



**HAL**  
open science

## Two-step CO<sub>2</sub> and H<sub>2</sub>O splitting using perovskite-coated ceria foam for enhanced green fuel production in a porous volumetric solar reactor

Anita Haeussler, Stéphane Abanades, A. Julbe, Julien Jouannaux, Bruno Cartoixa

► **To cite this version:**

Anita Haeussler, Stéphane Abanades, A. Julbe, Julien Jouannaux, Bruno Cartoixa. Two-step CO<sub>2</sub> and H<sub>2</sub>O splitting using perovskite-coated ceria foam for enhanced green fuel production in a porous volumetric solar reactor. *Journal of CO<sub>2</sub> Utilization*, 2020, 41, pp.101257. 10.1016/j.jcou.2020.101257. hal-02931720

**HAL Id: hal-02931720**

**<https://hal.science/hal-02931720>**

Submitted on 5 Nov 2020

**HAL** is a multi-disciplinary open access archive for the deposit and dissemination of scientific research documents, whether they are published or not. The documents may come from teaching and research institutions in France or abroad, or from public or private research centers.

L'archive ouverte pluridisciplinaire **HAL**, est destinée au dépôt et à la diffusion de documents scientifiques de niveau recherche, publiés ou non, émanant des établissements d'enseignement et de recherche français ou étrangers, des laboratoires publics ou privés.

# Two-step CO<sub>2</sub> and H<sub>2</sub>O splitting using perovskite-coated ceria foam for enhanced green fuel production in a porous volumetric solar reactor

Anita HAEUSSLER <sup>a</sup>, Stéphane ABANADES <sup>a\*</sup>, Anne JULBE <sup>b</sup>, Julien JOUANNAUX <sup>b</sup>, Bruno CARTOIXA <sup>c</sup>

<sup>a</sup> Processes, Materials and Solar Energy Laboratory, CNRS-PROMES, 7 Rue du Four Solaire, 66120 Font-Romeu, France

<sup>b</sup> Institut Européen des Membranes, IEM, UMR-5635, ENSCM, CNRS, Univ Montpellier, Place Eugène Bataillon, 34095 Montpellier cedex 5, France

<sup>c</sup> ALSYS-CTI, 382 avenue du Moulinas, 30340 Salindres, France

\* Corresponding author: Tel +33 (0)4 68 30 77 30

E-mail address: stephane.abanades@promes.cnrs.fr

**Declarations of interest: none**

## Abstract

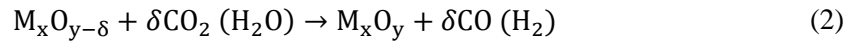
Solar thermochemical cycles offer a viable option for the production of green synthetic fuels from CO<sub>2</sub> and H<sub>2</sub>O. Two-step cycles using redox materials consist of a high-temperature reduction creating oxygen vacancies, followed by a re-oxidation step with an oxidant gas (CO<sub>2</sub> and/or H<sub>2</sub>O), resulting in CO and/or H<sub>2</sub> production. This study focuses on the thermochemical performance in a solar reactor of a new kind of composite reactive material: reticulated ceria foam with uniform perovskite coating, forming a dual-phase layered heterostructure. La<sub>0.5</sub>Sr<sub>0.5</sub>Mn<sub>0.9</sub>Mg<sub>0.1</sub>O<sub>3</sub> (LSMMg) was selected as perovskite coating due to its high fuel productivity and thermochemical stability upon cycling. The perovskite coating improves the reduction step by increasing the reduction extent reached by the reactive material. The results revealed significant enhancement of oxygen exchange in the dual-phase composite material during reduction compared to individual components. The enhanced reduction extent had a beneficial effect on the oxygen release rate and the total amount of fuel produced by CO<sub>2</sub> and H<sub>2</sub>O splitting, whereas an adverse impact on the peak rate during H<sub>2</sub>/CO evolution was noticed. Decreasing the reduction pressure allowed enhancing the non-stoichiometric oxygen extent, while the re-oxidation extent increased with the inlet oxidant molar fraction. With suitable operating conditions (reduction at 0.100 bar and oxidation in 100% CO<sub>2</sub>), the LSMMg-coated ceria foam produced a higher amount of fuel but with lower fuel production rate in comparison with pure ceria foam. This study points out the beneficial effects of composite redox materials consisting of LSMMg-coated ceria foam in enhancing the oxygen exchange capacity of ceria for solar fuel production.

**Keywords:** Solar fuel, CO<sub>2</sub> valorization, water-splitting, perovskite, ceria foam, solar energy, hydrogen-syngas.

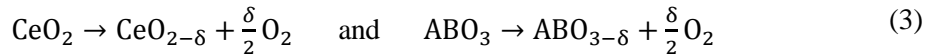
## 1. Introduction

One of the biggest challenges of the 21<sup>st</sup> century is to transition from fossil fuel energy to renewable energy systems. Among the renewable resources, the sunlight seems especially interesting, because it

is widely available, inexhaustible and free [1]. The harvestable solar energy potential is 50000 EJ per year [2], while the world energy consumption reached 504 EJ per year [3]. Concentrated solar power can be used to drive high temperature thermochemical processes that produce green energy vectors, with low carbon emission. Furthermore, no intermediate electricity production is required as the process directly converts heat to chemical fuels, thereby allowing a high theoretical energy conversion efficiency. It is also necessary to develop technologies that beneficially use CO<sub>2</sub> to produce valuable products and recycle waste CO<sub>2</sub> streams back into the economy. Converting CO<sub>2</sub> into useful value-added sustainable fuels is an attractive route for reducing carbon emissions. Thermochemical cycles using non-stoichiometric oxides can produce CO, H<sub>2</sub>, or syngas, based on carbon dioxide and water dissociation. The first step (reaction 1) consists of partial thermal reduction at high temperature supplied by solar energy. Oxygen vacancies are created in the oxide lattice leading to pure oxygen release. The second step (reaction 2) is a re-oxidation reaction of the reactive partially-reduced material with an oxidant gas (H<sub>2</sub>O and/or CO<sub>2</sub>), resulting in the production of H<sub>2</sub> and/or CO. The syngas can be further converted to synthetic liquid fuels via catalytic processes. CO and H<sub>2</sub> can also be produced simultaneously, but their separate production is more practical since the individual gases can then be mixed in suitable proportions (controlled H<sub>2</sub>/CO ratio) for the considered synthesis. Furthermore, CO can be shifted to H<sub>2</sub> if H<sub>2</sub>-rich gas is targeted.



Ceria (CeO<sub>2</sub>) has been widely considered as the state of art material for thermochemical cycles, due to its thermodynamically favorable oxidation, fast reaction rate as well as good thermal stability. Notwithstanding, ceria requires high reduction temperatures to achieve significant reduction extent [4–7]. To overcome this issue, numerous perovskite-based materials (ABO<sub>3</sub> where A and B sites are occupied by cations with coordination of 12 and 6, respectively) have been proposed for thermochemical cycles due to their high oxygen exchange capacity at lower temperature than ceria [8–11]. The corresponding CO<sub>2</sub> splitting specific reactions for ceria and perovskites can be written as follows:



Lanthanum cobalt perovskites have been investigated due to their high reduction extent. However, both their re-oxidation extent and production stability are low, making them unsuitable for thermochemical applications requiring numerous consecutive redox cycles [11]. Strategies for doping the lanthanum cobalt perovskites with Ca<sup>2+</sup> or Sr<sup>2+</sup> in A-site or with Cr and Fe in B-site have been investigated, but in all cases the fuel production decreased over cycles [10–16]. Lanthanum-manganite perovskites doped with strontium (A-site substitution) have been extensively studied for assessing their thermochemical performance. The Sr<sup>2+</sup> cation in A-site leads to an increase of the Mn oxidation state for electronic neutrality that allows increasing the reduction extent. The optimum Sr stoichiometry in the lanthanum manganite perovskites is assumed to be in the range 0.3–0.5 [15, 17–24]. Another A-site dopant for lanthanum manganite perovskites is Ca<sup>2+</sup>. Similarly to Sr<sup>2+</sup> cation, it increases the reduction extent, although a decrease of the re-oxidation extent was also reported [13, 25–28]. Among the various investigated formulations, La<sub>0.5</sub>Sr<sub>0.5</sub>Mn<sub>0.9</sub>Mg<sub>0.1</sub>O<sub>3</sub> (LSMMg) was highlighted as a promising reactive material due to its noticeable fuel production capacity combined with enhanced thermal stability arising from the presence of Mg<sup>2+</sup> that alleviates sintering [25, 29].

In addition to the research of suitable materials formulations to perform thermochemical cycles, different reactor prototypes were also designed and investigated in the literature. Thirteen

thermochemical cycles with a ceria reactive coating on inert zirconia foam were performed using a 40 kW<sub>th</sub> solar furnace. An average H<sub>2</sub> production per cycle of 2.1 mL/min was obtained [30, 31]. Hathaway et al. [32] produced 360 mL/min of CO in isothermal conditions (1477°C) in a 4.4 kW solar reactor with ceria as reactive material in a fixed bed. The solar-to-fuel conversion efficiency achieved a value of 1.64% with a gas-phase heat recovery. In a monolithic reactor irradiated by artificial light using ceria foam as reactive material, 500 cycles were performed resulting in peak and average solar-to-fuel efficiencies of 3.53% and 1.73%. With a reduction temperature of 1500°C under a pressure of 10 mbar and an oxidation temperature of 800°C, the efficiency reached 5% [33]. Another reactor concept consists of counter rotating ring in which an instant solar-to-fuel efficiency of 1.7% and peak CO production rate of 100 mL/min were obtained [34–36]. An indirectly-irradiated solar tubular reactor with packed bed particles was developed and tested using ceria granules prepared from cork templates, yielding a CO peak production rate of 1.9 mL/min/g (reduction step at ~1400°C and atmospheric pressure) [37]. A new monolithic solar reactor to perform two-step thermochemical cycles was designed in PROMES-CNRS (France). The impact of the operating conditions during thermochemical cycling of reticulated ceria foams as reactive materials was highlighted. Either a decrease of pressure or an increase of temperature during the reduction step increased the maximum reduction extent reached in the porous structure, and thus the fuel production yield during the oxidation step. The yield of the oxidation step with ceria was enhanced by applying either a low oxidation temperature or a high oxidant molar fraction [38, 39].

In this work, in order to promote the reduction extent in comparison with pure ceria, metal oxide dual-phase composites of LSMMg-CeO<sub>2</sub>, in the form of reticulated foams, have been experimentally investigated for thermochemical redox reactions in a solar reactor for the first time. The increase of the oxygen exchange capacity and reaction kinetics in non-stoichiometric solid oxides is required to improve the thermochemical performance of most redox materials such as ceria for solar-to-fuel production. This study aims to investigate the thermochemical performance of a ceria foam coated with La<sub>0.5</sub>Sr<sub>0.5</sub>Mn<sub>0.9</sub>Mg<sub>0.1</sub>O<sub>3</sub> in a newly developed solar reactor under realistic high-flux solar irradiation conditions. Such heterogeneous structures have never been investigated to date for solar thermochemical fuel production, and their shaping and testing as reticulated foams was never addressed. Significant efforts have thus been achieved to incorporate such materials in a reactor prototype and test the performance. The ceria foam coated with LSMMg was expected to combine the advantages of ceria fast and complete re-oxidation, with the high reduction extent of LSMMg [40].

## 2. Experimental set-up and methods

### 2.1 Materials synthesis and characterization

The details concerning materials synthesis and characterization are available in the supporting information. The perovskite powder was synthesized using a modified liquid-phase Pechini process, as described previously [29]. The obtained perovskite powder (LSMMg) was then used as starting material for preparing the ceramic suspension able to coat uniformly the ceria foams (20 ppi) provided by Alsys-CTI [38]. The perovskite powder was dispersed in water (45 wt %) using a polymethacrylate dispersing agent (DARVAN C-N®) and polyvinyl alcohol (Rhodoviol, 2 wt%) as a binder/plasticizer. A SpeedMixer® (DAC 150.1 FVZ-K) was used to prepare fluid, uniform, stable and smooth slurries, suitable for casting. These suspensions were used to coat the surface of ceria foams (20 ppi) with a consolidated LSMMg layer. A set of 5 foams parts was used, comprising 4 rings and one disk (45 mm outer diameter, 20 mm inner diameter and 10 mm height) and all parts were weighted before and after the deposition and firing steps. A dip coating unit (Chemat Technology Dip Master 201) was used to perform the coating with a good repeatability. Ceramic parts were soaked into the LSMMg slurry for 90 seconds. The coated foams went through a multi-step thermal treatment with a final sintering step at 1500 °C for 8 h (2°C/min ramp). The sintered samples were weighted again in order to calculate the

effective amount of LSMMg coated at the surface of ceria foams that was in the range 7.7- 11.4 wt% (Table S1). Good adhesion of the perovskite coating on the ceria foam was confirmed by sonication tests. Moreover, the absence of interaction between the perovskite coating and the ceria foam was confirmed by X-Ray Diffraction (Figure S1).

The ceria foam microstructure (before and after perovskite coating) was also characterized by Scanning Electron Microscopy (SEM, Hitachi S-4800). The foam struts are composed of micron-sized grains in the range 3-10  $\mu\text{m}$  forming an interconnected macroporous network (Figure S2). The reticulated porous foams (20 ppi cell density) thus exhibit both millimetric scale open cells for solar radiation volumetric absorption and fine granular microstructure (micron-sized grains and interconnected pores) within the foam struts for favorable oxidation reaction. The black perovskite layer also promotes solar radiation absorption in comparison with uncoated white ceria (although non stoichiometric ceria turns to black during reduction). The thickness of the LSMMg layer (composed of fine micrometric grains) at the ceria foam surface is estimated to be  $\sim 10 \mu\text{m}$  (Figure 1). The distribution of elements in the coated foam has been analyzed by EDS mapping (Zeiss Evo HD15) and results are provided in Figure S3.

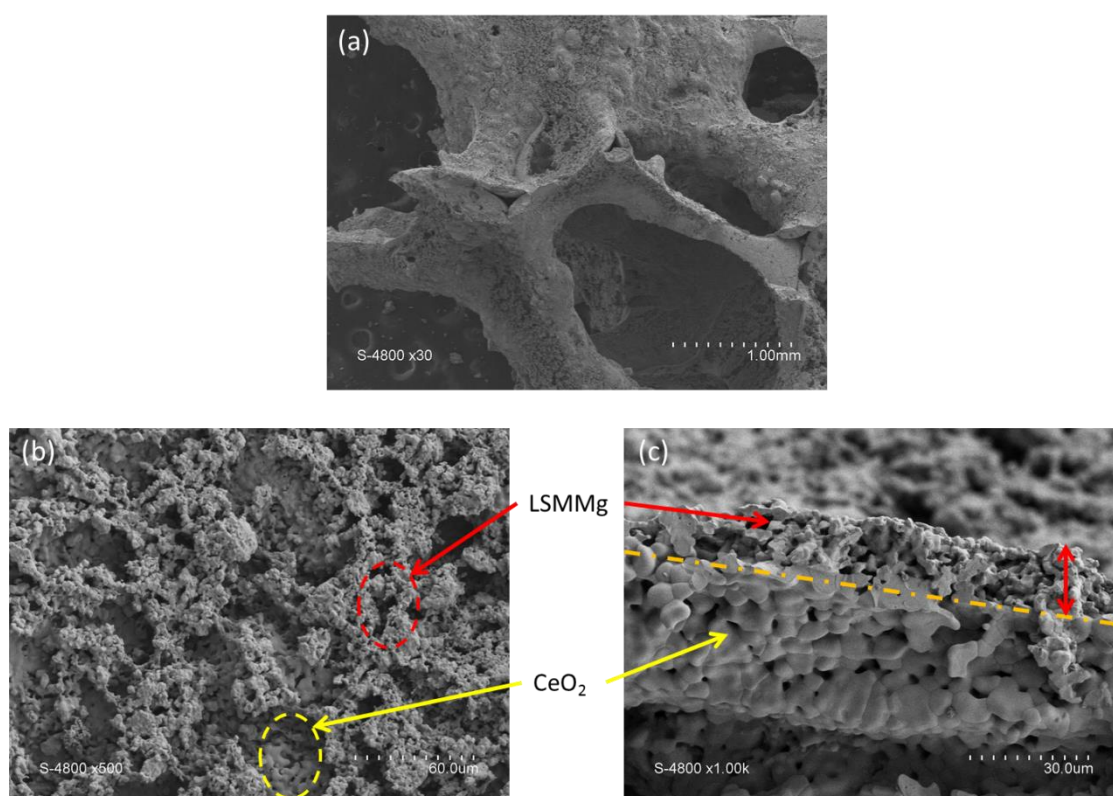


Figure 1. SEM micrographs of LSMMg-coated  $\text{CeO}_2$  foam (after sintering at  $1500^\circ\text{C}$  for 8h): (a) general view, (b) surface view and (c) cross-section view.

The  $\text{CO}_2$ -splitting redox activity of the individual materials in two-step cycles was experimentally investigated via temperature-programmed thermogravimetric analysis in a controlled atmosphere (TGA, Setaram Setsys Evo 1750 offering a measuring resolution equivalent to a microgram). The powder samples (about 105 mg) were placed inside a platinum crucible (0.1 mL) and were subjected to two thermochemical cycles comprising the thermal reduction step in flowing Ar (99.999% purity,  $20 \text{ mL min}^{-1}$ ) and the oxidation step in  $\text{CO}_2$  atmosphere (50%  $\text{CO}_2$  in Ar,  $\text{CO}_2$  flow rate of  $10 \text{ mL min}^{-1}$ ). The gas flowed from the top to the bottom of the tubular reaction chamber. Before each test, the furnace chamber was purged thanks to a primary vacuum circuit and then filled with argon to eliminate air in the reaction zone. A Pt-Rh thermocouple (type B) at the back of the crucible controlled the

temperature inside the experimental chamber. The reduction was carried out at 1400°C (heating rate of 20 °C min<sup>-1</sup>, 45 min plateau), in flowing Ar, and the oxidation step at 1050°C (cooling rate of 20 °C min<sup>-1</sup>, 60 min plateau), in flowing CO<sub>2</sub> stream mixed with Ar. During the oxidation step, CO<sub>2</sub> was injected once the targeted reaction temperature was reached, whereas the reduction step started during sample heating and continued during the temperature plateau. The sample mass variation during the cycle steps was measured: it was a mass loss in the case of thermal reduction (due to O<sub>2</sub> release) and a gain during oxidation with CO<sub>2</sub> (due to oxygen atoms replenishment from CO<sub>2</sub> gas, producing CO). The O<sub>2</sub> and CO production yields were then determined from these mass variations.

In addition, the thermochemical redox activity of the perovskite-coated ceria foams was experimentally studied in a solar reactor heated by real concentrated solar radiation, as described in the next section.

## 2.2 Solar reactor configuration

A schematic representation of the solar reactor is presented in Figure 2. The solar reactor is designed to perform two-step thermochemical cycles with reactive monolithic structures [38]. The solar experiments were carried out using the medium size solar facilities of PROMES-CNRS laboratory (France). The solar concentrating system consists of a 2m-diameter parabolic dish concentrator coupled with a sun-tracking heliostat. The solar reactor is composed of a water-cooled stainless-steel outer shell and it is sealed at the front with a quartz window to let the sunlight entering in the solar absorber cavity. The insulated cavity is a 60x50 mm alumina tube closed by an alumina cover with 18 mm-diameter aperture. The reticulated foams (pure CeO<sub>2</sub> and LSMMg-coated foam) are composed of 4 piled rings (45 mm outer diameter, 20 mm inner diameter and 10 mm height) and one bottom disk, forming a cylindrical cavity for enhanced solar radiation absorption (Figs. S4-S5). About 80 g of reactive material is loaded in the cavity (Fig. S5). The temperature is measured at different places of the reactor thanks to three B-type thermocouples (T1, T2 and T3) and a solar-blind pyrometer. The pressure is monitored with three pressure sensors at gas inlets and within the cavity (not represented on the illustration).

During the reduction step, the reactor was heated by the solar radiation until reaching the desired temperature (1400°C at T1) by opening gradually the shutter positioned below the reactor. An argon flow (99.999% purity with [O<sub>2</sub>] < 2 ppm) of 1 NL/min sweeps the glass window while another argon flow of 0.2 NL/min enters from the lateral side of the reactor directly in the cavity. Both argon flows exit from the single outlet at the reactor bottom and evacuate the released oxygen. A fraction of the output gas was analyzed by a trace oxygen electrochemical analyzer (Systech) to measure continuously the proportion of oxygen in the gas output. In the case of reduction step performed under low pressure in flowing Ar, a vacuum pump was settled at the reactor outlet. The operating pressure was decreased during the reduction step only (~0.1 bar) in order to study the effect of total pressure on both the reduction extent and associated fuel production yield during oxidation. For the oxidation step, the pump was not used and the pressure was increased after the reduction step by Ar filling. During both steps, continuous gas flow was maintained through the foam (inducing negligible pressure drop), in order both to favor gas-phase mass transfer and transport of gas products to the outlet. Such continuous removal of products shifts reactions to the products side and favors reaction completion. When the reduction becomes low enough (i.e. O<sub>2</sub> concentration falls below 500 ppm), the solar power input is removed and the reactor starts to cool down. At the desired temperature for oxidation step (typically 1050°C), the argon flows are modified according to the desired operational parameters and the oxidant gas (CO<sub>2</sub> or H<sub>2</sub>O) is injected in the cavity (liquid water is steadily vaporized when entering the heated reactor and steam is transported by the Ar carrier gas to the cavity). To perform experiments with varying mole fractions of either CO<sub>2</sub> or H<sub>2</sub>O in the feed, Ar is used as a second/diluent gas. Right after the fuel production rate increases promptly to reach a peak, and then decreases slowly. The different gas and liquid flows are regulated thanks to mass flow controllers

(MFC, Brooks Instruments model SLA5850S). The  $\text{CO}_2$  and  $\text{CO}$  concentrations at the reactor outlet are analyzed online by NDIR sensors (MGA3000). When using  $\text{H}_2\text{O}$  steam as oxidant gas, the water contained in the outlet gas is first condensed in a bubbler and a desiccant column, and a sample is then analyzed continuously for  $\text{H}_2$  concentration measurement by a catharometer based on thermal conductivity detection (calibrated for  $\text{Ar}/\text{H}_2$  binary mixture). The different gas yields are calculated by integrating the gas production rates over the experiment duration. All the instantaneous measured data are registered thanks to an automated acquisition system.

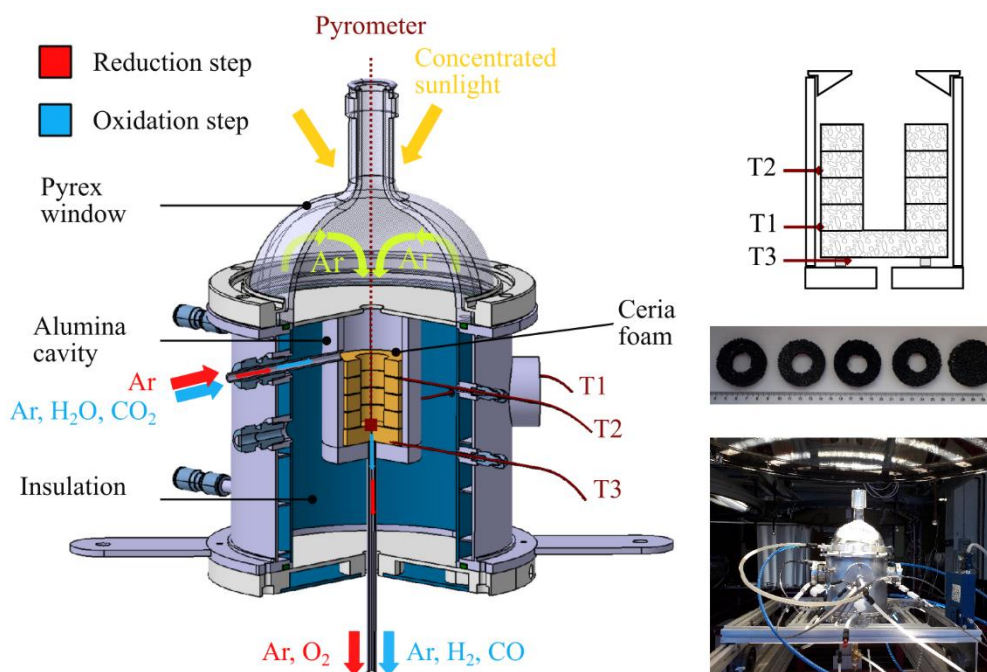


Figure 2. Scheme of solar reactor with cavity shape (top right), foam picture composed of 4 rings and one bottom disk (middle) and reactor picture during solar test (bottom)

### 3. Results and discussion

#### 3.1 Thermochemical cycling performance

Thermochemical performance of redox materials during solar-driven  $\text{H}_2\text{O}$  and  $\text{CO}_2$  splitting cycles were experimentally determined. Solar-to-fuel conversion efficiency of ceria is limited due to its moderate reduction extent at reasonable reduction temperatures (up to  $1400^\circ\text{C}$ ). In contrast, perovskites offer higher oxygen exchange capacity and have thus been proposed as alternative materials for  $\text{H}_2\text{O}$  and  $\text{CO}_2$  splitting. However, their re-oxidation step is slow and incomplete due to thermodynamic limitation, contrary to ceria oxidation which is thermodynamically more favorable. Figure 3 presents the thermogravimetric analysis (TGA) of individual ceria and LSMMg powders with the associated  $\text{O}_2$  and  $\text{CO}$  productions summarized in Table 1. The reduction extent reached at  $1400^\circ\text{C}$  during the first cycle by LSMMg ( $269 \mu\text{mol/g}$ ) is almost five times higher than that of ceria ( $55 \mu\text{mol/g}$ ). However, the re-oxidation extent of LSMMg for the first cycle is low (40%) and still incomplete after one hour dwell at  $1050^\circ\text{C}$ , due to slow kinetics. In contrast, oxidation rates for ceria are extremely fast in comparison with LSMMg. Both materials show stable fuel production yields during cycling. Thus, LSMMg displays a favorable oxygen exchange capacity during reduction steps whereas ceria shows favorable reaction kinetics during oxidation steps. To take advantages of both materials characteristics, i.e. enhanced reduction extent combined with favorable oxidation rate, a heterogeneous composite material structure consisting of LSMMg-coated ceria foam has been developed and tested under real concentrated solar radiation.

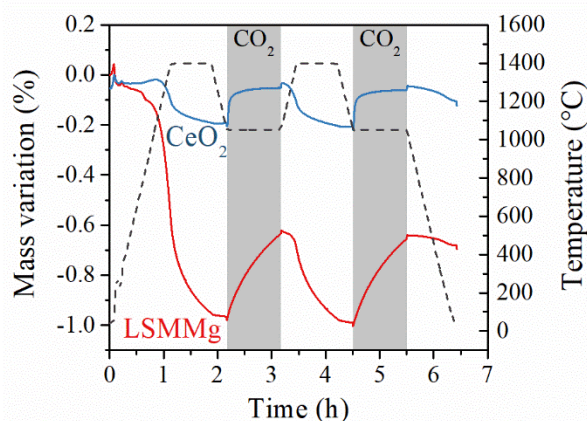


Figure 3. Thermogravimetric analysis (TGA) of LSMMg and CeO<sub>2</sub> powders during redox cycling

Table 1. O<sub>2</sub> and CO production yields along with associated re-oxidation extents obtained during the thermogravimetric analysis of CeO<sub>2</sub> and LSMMg individual powders, submitted to successive redox cycles.

	1 <sup>st</sup> cycle				2 <sup>nd</sup> cycle			
	O <sub>2</sub> production yield (μmol/g)	CO production yield (μmol/g)	Re-oxidation extent	Maximum CO production rate (mL/g/min)	O <sub>2</sub> production yield (μmol/g)	CO production yield (μmol/g)	Re-oxidation extent	Maximum CO production rate (mL/g/min)
CeO <sub>2</sub>	55	95	86%	0.89	54	98	91%	0.98
LSMMg	269	214	40%	0.29	111	215	97%	0.21

In order to evaluate the beneficial impact of LSMMg coating on the ceria foam, the performance of a LSMMg coated ceria foam (LSMMg-CeO<sub>2</sub>) were compared with those of a pure ceria foam with same cell density (20 ppi). First, a thermochemical cycle was performed in the solar reactor with the following conditions: reduction at 1400°C (T1) under atmospheric pressure followed by an oxidation step starting at ~1000°C (free cooling without solar power input) under 25mol% of CO<sub>2</sub> as oxidant gas. These conditions are referred in the following as “reference conditions”. Figure S6 presents the O<sub>2</sub> and CO production rates evolutions along with temperature profiles for the thermochemical cycle performed at these conditions. The O<sub>2</sub> production yield is twice higher for LSMMg-CeO<sub>2</sub> foam (166 μmol/g) than for pure CeO<sub>2</sub> foam (86 μmol/g). The LSMMg coating thus favors the reduction extent, which can be explained by the enhanced reduction extent of the perovskite material. Furthermore, a potential synergetic improvement of oxygen exchange in the composite material is revealed during the reduction step, in comparison with individual components. This is attributed to the thin LSMMg coating that boosts the oxygen exchange capacity of the composite material, in comparison with ceria. Accounting for the mass fraction of each material in the foam composite (10% LSMMg, 90% CeO<sub>2</sub>), the expected theoretical O<sub>2</sub> yield would be ~119 μmol/g for LSMMg-CeO<sub>2</sub> (see Supporting Information for detailed calculation), which is lower than the value measured experimentally, thereby suggesting a synergistic effect of the composite layered structure. This demonstrates the promotional effect of LSMMg in the O<sub>2</sub> releasing step. However, the re-oxidation of LSMMg-CeO<sub>2</sub> foam is less favorable compared with pure CeO<sub>2</sub> foam. Indeed, the amount of CO produced (145 μmol/g), the peak CO production rate (0.8 mL/g/min) and the re-oxidation extent (44%) of LSMMg-CeO<sub>2</sub> foam are lower than those measured for pure CeO<sub>2</sub> foam (186 μmol/g, 1.5 mL/g/min, 100%, respectively). Furthermore, the time to reach 90% of the total CO amount produced ( $\tau_{90}$ ) reaches 7.4 min for LSMMg-CeO<sub>2</sub> foam (cycle #1), against 5.7 min for pure CeO<sub>2</sub>

foam. Contrary to the reduction step, the oxidation step is therefore hindered by the LSMMg coating which may act as a diffusion barrier limiting the access of oxidant gas species to the ceria bulk.

Figure S7 presents the two first thermochemical cycles of LSMMg-CeO<sub>2</sub> foam. Both the O<sub>2</sub> and CO production yields dropped between the first and second cycle. This can be explained by the low re-oxidation extent of the first cycle (44%) impeding full material re-oxidation. During the second cycle, the starting oxidation temperature was decreased down to 900°C because a lower oxidation temperature thermodynamically favors the oxidation step. The CO yield remained weak due to a lower reduction extent but the re-oxidation extent slightly increased up to 50%. It is thus necessary to further improve the re-oxidation extent to increase the thermochemical performance of the LSMMg-CeO<sub>2</sub> foam. The thin perovskite layer at the ceria surface hinders the oxidant gas access to the reactive ceria, which mostly explains the partial re-oxidation observed during the two first cycles. Increasing the oxidant partial pressure can be a suitable option to favor both the reactant diffusion and reaction kinetics, and to promote the re-oxidation extent of the composite material.

### 3.2 Improvement of the fuel production capacity

In order to improve the re-oxidation extent of LSMMg-CeO<sub>2</sub>, some relevant operating conditions, highlighted in a previous study [38], were investigated during additional cycles. In total, the foam underwent 10 cycles, as presented in Figure 4. The operating conditions of each cycle along with O<sub>2</sub> and fuel production yields are reported in Table 2. The total amount of H<sub>2</sub> and CO produced reached 1.1 L (3 cycles) and 3.5 L (7 cycles), respectively. It is important to underline that the LSMMg-CeO<sub>2</sub> foam underwent these 10 cycles, corresponding to 26 h of continuous on-sun operation, without any performance decline.

Table 2: O<sub>2</sub> and fuel production yields for the composite LSMMg-CeO<sub>2</sub> foam along with the operating conditions (total foam mass =88.2178 g)

Cycle #	Reduction step				Oxidation step				
	T1 <sub>red</sub>	Reduction pressure	O <sub>2</sub> production yield	T1 <sub>ox</sub>	Oxidant (molar fraction)	Oxidant flow rate/total flow rate	Fuel production yield	Maximum fuel production rate	τ <sub>90</sub>
	(°C)	(bar)	(μmol/g)	(°C)		(NL/min)	(μmol/g)	(mL/g/min)	(min)
1	1398	0.871	166	1011-777	CO <sub>2</sub> (0.25)	0.40/1.60	145	0.8	7.4
2	1403	0.867	89	904-688	CO <sub>2</sub> (0.25)	0.40/1.60	89	0.7	6.2
3	1411	0.101	222	1045-988	CO <sub>2</sub> (1.00)	2.00/2.00	387	4.6	5.8
4	1399	0.910	87	1040-671	H <sub>2</sub> O (0.17)	0.25/1.45	149	0.2	13.1
5	1406	0.098	206	1061-757	CO <sub>2</sub> (1.00)	2.00/2.00	359	4.3	4.6
6	1403	0.873	89	1008-753	CO <sub>2</sub> (1.00)	2.00/2.00	172	2.1	3.8
7	1409	0.100	203	1034-781	H <sub>2</sub> O (0.24)	0.80/3.30	234	1.4	6.1
8	1407	0.910	72	959-615	H <sub>2</sub> O (0.50)	0.80/1.60	166	1.1	7.5
9	1407	0.102	202	1050-774	CO <sub>2</sub> (0.67)	2.00/3.00	298	3.6	4.4
10	1407	0.096	153	1041-680	CO <sub>2</sub> (1.00)	1.00/1.00	344	2.3	7.2

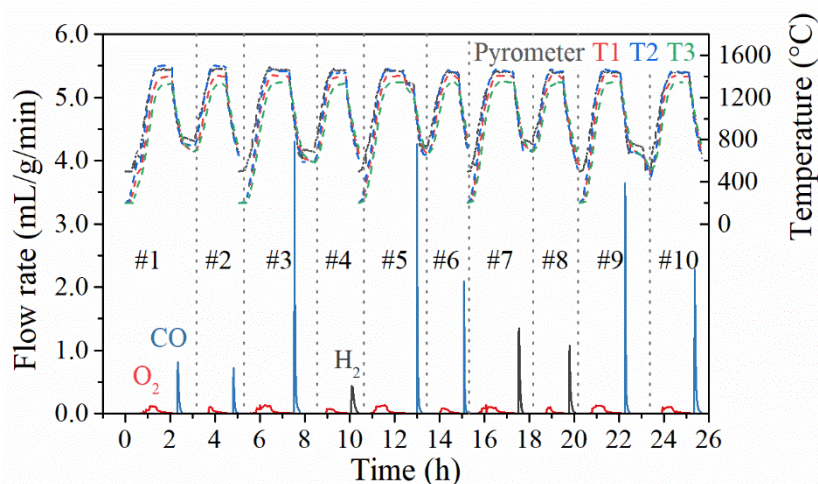


Figure 4. Evolution of  $O_2$  and  $CO$  production rates during ten successive thermochemical cycles performed with the composite  $LSMMg-CeO_2$  foam.

Figure 5 presents the amounts of  $O_2$  and  $CO$  or  $H_2$  produced along with the re-oxidation extent, the reduction pressure and the oxidant molar fraction. A low pressure ( $\sim 100$  mbar) during the reduction step increases the reduction extent because oxygen release is thermodynamically favored by a low oxygen partial pressure. Moreover, the use of low reduction pressure induces a higher fuel production yield, with for example an increase from  $172 \mu\text{mol/g}$  (cycle #6) to  $359 \mu\text{mol/g}$  (cycle #5) with a decrease of the reduction pressure from 0.873 bar to 0.098 bar. It seems that pressure reduction has a stronger effect on the performance of  $LSMMg-CeO_2$  foam than on those of  $CeO_2$  foam. Indeed, it leads to an improvement of 130% of the reduction extent for  $LSMMg-CeO_2$  foam, while a non-stoichiometric increase from  $\delta=0.031$  to 0.044 for pure ceria foam was previously reported [38] for a similar pressure reduction, corresponding only to 44% improvement. In addition, the pumping energy penalties only represent 0.27 % of the total energy input, which is negligible accounting for the beneficial increase of the reduction extent. Thus, using pumping to reduce the oxygen partial pressure during the reduction step is highly beneficial for system performance. Cycles #3 and #5 were performed practically under the same conditions (reduction at low pressure, re-oxidation in pure  $CO_2$ ), which confirms the results repeatability since the obtained  $O_2$  and  $CO$  production yields are very similar.

Besides, the re-oxidation extent is directly correlated with the inlet oxidant molar fraction. A  $CO_2$  molar fraction of 0.25 leads to an average re-oxidation extent of 47% versus 96% for a  $CO_2$  molar fraction of 1.00. It should be noted, that the cycles #8 and #10 feature an apparent re-oxidation extent above 100%, which is due to the incomplete re-oxidation during the previous cycle. The re-oxidation extent is also improved by increasing the  $H_2O$  molar fraction. The  $H_2O$  molar fraction cannot be increased as much as the  $CO_2$  molar fraction due to technical limitations. However, a  $H_2O$  molar fraction of 0.50 is sufficient to reach complete re-oxidation extent, as shown in cycle #8.

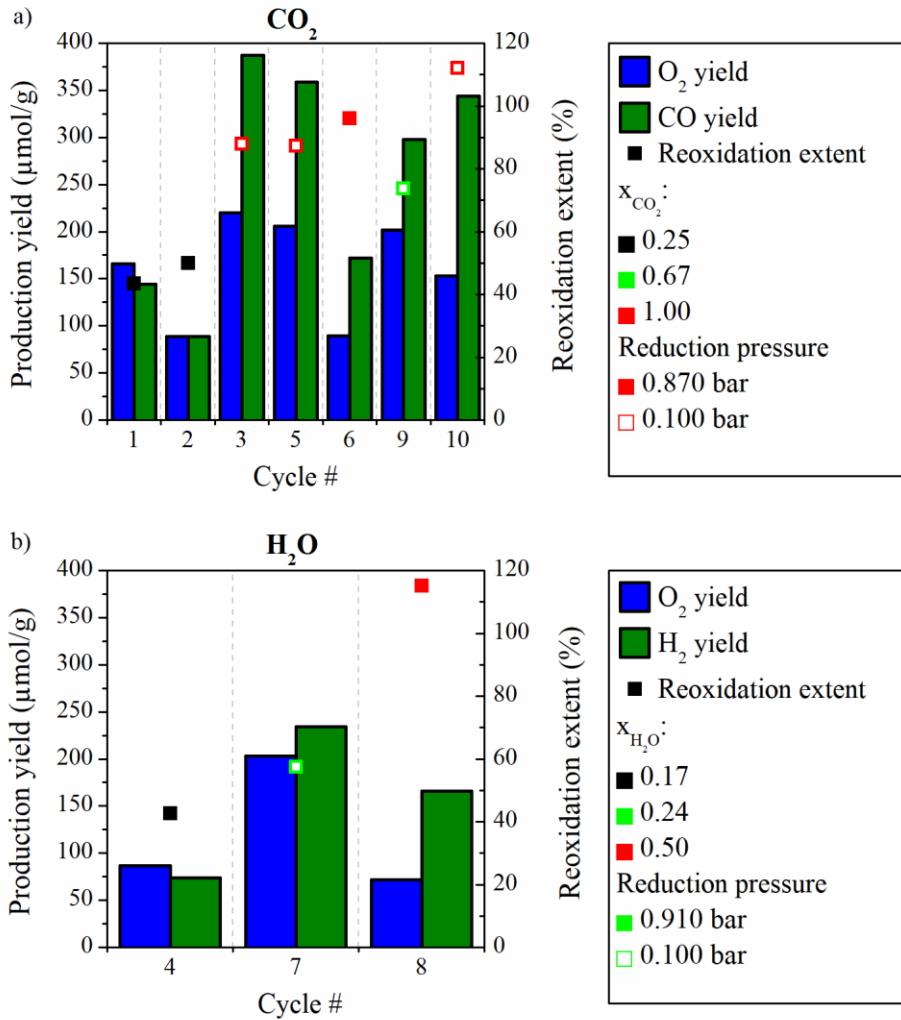


Figure 5. Fuel production yields and re-oxidation extents with the different operating conditions for a) CO<sub>2</sub> oxidant gas and b) H<sub>2</sub>O oxidant gas; the bar color represents the gas produced, the square color shows the oxidant molar fraction and hollowed symbol indicates a low pressure during the reduction step

The inlet CO<sub>2</sub> flow rate during the oxidation step was also investigated (cycle #3 and cycle #10 with 2 L/min and 1 L/min, respectively, during the oxidation step with a CO<sub>2</sub> molar fraction of 1.00). Figure 6 shows that a two-fold decrease of the inlet gas flow rate (CO<sub>2</sub>) leads to a similar two-fold decrease of the peak CO production rate (from 4.3 mL/g/min to 2.3 mL/g/min). The CO<sub>2</sub> outlet flow rate increases with the decrease of the CO production rate until it reaches the same value than the CO<sub>2</sub> inlet flow rate, meaning oxidation completion. Furthermore,  $\tau_{90}$  is also affected by the CO<sub>2</sub> flow rate:  $\tau_{90}$  equals 7.2 min for 1 L/min of inlet CO<sub>2</sub> flow rate against 5.8 min for 2 L/min. Thus, increasing the CO<sub>2</sub> flow rate promotes the global rate of the oxidation process, although the intrinsic kinetics depends on the temperature and species concentration (CO<sub>2</sub> mole fraction). Therefore, the effect of CO<sub>2</sub> flow rate must be analyzed on a thermodynamic viewpoint, since it basically affects the CO/CO<sub>2</sub> ratio in the reaction zone and a thermodynamically-favored oxidation reaction is related to a low CO/CO<sub>2</sub> ratio. Since the important performance metrics are both the overall fuel yield of the solid material and the production rate (affecting the time required to convert the maximum possible quantity of CO<sub>2</sub>), the CO<sub>2</sub> flow-rate should be considered as a possible control parameter for optimizing the process. However, a low inlet CO<sub>2</sub> flow rate has beneficial impact on CO<sub>2</sub> conversion (CO<sub>2</sub> outlet flow rate was calculated from the produced CO flow rate as follows:  $F_{CO_2, out} = F_{CO_2, in} - F_{CO, out}$ ). For example, a CO<sub>2</sub> conversion extent and peak CO<sub>2</sub> conversion of 3.4% and 20.1% respectively, were obtained with

$Q_{\text{CO}_2}=1$  L/min, compared with 2.3% and 19.0% with  $Q_{\text{CO}_2}=2$  L/min. This is because the limiting factor at lab-scale is the amount of reactive solid material loaded in the reactor. Given the low  $\text{CO}_2$  conversion achieved, one can infer that  $\text{CO}_2$  in the feed is in high excess with respect to the maximum yield possible by the solid at the specific conditions and it is expected that  $\text{CO}_2$  conversion will drop by increasing the  $\text{CO}_2$  flow rate. The amount of converted  $\text{CO}_2$  is fixed by the amount of redox material and its reduction extent ( $\delta$  in Eq. 4). Given that the redox capacity is finite, the higher the amount of fed  $\text{CO}_2$ , the lower the global  $\text{CO}_2$  conversion. The  $\text{CO}_2$  conversion will need to be optimized in a large-scale reactor to minimize the amount of unreacted  $\text{CO}_2$  in the outlet gas.

The CO production yield is also higher when increasing the  $\text{CO}_2$  flow rate (390  $\mu\text{mol/g}$  with  $Q_{\text{CO}_2}=2$  L/min vs. 344  $\mu\text{mol/g}$  with  $Q_{\text{CO}_2}=1$  L/min). Since the oxidant feeding is continuous, the gas-phase mass transfer is promoted when increasing the gas flow rate, which favors the gaseous oxidant access to the reactive surface and avoids any lack of reactant that may hinder the reaction (because of low local  $\text{CO}_2$  concentration at the surface). Moreover, internal gas diffusion within the porous struts of the foam is also favored by high surface  $\text{CO}_2$  concentrations, arising from the gas flow-rate increase. This is especially true for the coated ceria foam because the oxidant first needs to diffuse through the perovskite coating before reaching the underlying bulk ceria reactant. Furthermore, high gas flow rates also favor gas products dilution and their continuous removal from the reaction site, thus shifting the equilibrium to the products side and promoting the oxidation thermodynamic driving force. Conversely, the gas residence time in the porous solid foam (or solid/gas contact time) is inherently decreased by increasing the flow-rate (it is about 4 s for 1 NL/min), but this is not a limiting factor because the gas feeding is continuous and fresh gaseous reactant is thus always available to react at the solid surface. It must be pointed out that the redox system is not a catalytic reactor, hence the contact time does not affect the global  $\text{CO}_2$  conversion, given that the amount of  $\text{CO}_2$  converted is limited only by the solid material reduction extent ( $\delta$ ).

In summary, a high inlet  $\text{CO}_2$  flow rate thus enhances the CO production rate and yield. This can be explained by both a better access of the oxidant gas to the reactive surface and by CO product dilution (lower CO/ $\text{CO}_2$  ratio). The favorable oxidation with higher inlet  $\text{CO}_2$  can be explained by a lower peak CO/ $\text{CO}_2$  ratio (0.23 for 2 L/min vs. 0.25 for 1 L/min of inlet  $\text{CO}_2$ ). Indeed, a lowered CO/ $\text{CO}_2$  ratio (by increasing  $\text{CO}_2$  flow-rate) thermodynamically shifts the oxidation reaction to the side of CO formation.

However, the decrease of the  $\text{CO}_2$  molar fraction by increasing total inlet gas flow has adverse impact on kinetics. Indeed, cycle #9 was carried out with a total gas flow of 3 L/min but a  $\text{CO}_2$  molar fraction of 0.67 (i.e.  $\text{CO}_2$  flow rate was kept at 2 L/min as for cycle #3, but 1 L/min of Ar was added). Increasing the total gas flow was expected to improve CO product dilution and gas products removal, thus favoring equilibrium shift to the products side, in turn promoting the overall oxidation rate. However, the resulting lower  $\text{CO}_2$  molar fraction impeded the total re-oxidation and hindered the kinetics, leading to a decreased CO production rate (3.6 mL/g/min) compared with cycle #3 (4.6 mL/g/min). Thus a high total gas flow rate associated with a high oxidant molar fraction should be used. However, the total gas flow rate should be kept at reasonable value to avoid useless energy penalties due to sensible inert gas heating and downstream gas separation associated with a low  $\text{CO}_2$  conversion extent.

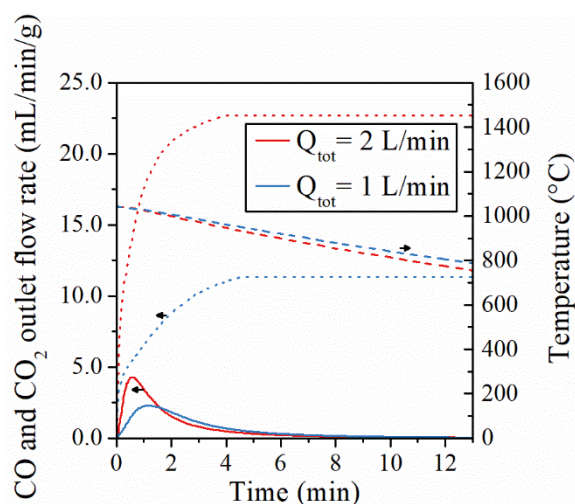


Figure 6. CO production rate (solid lines) along with CO<sub>2</sub> output flow rate (dotted lines) and temperature (dashed lines) for a CO<sub>2</sub> inlet flow-rate of 1 L/min (cycle #10) and 2 L/min (cycle #3) with a constant CO<sub>2</sub> molar fraction of 1.00.

### 3.3 Comparison of the CO<sub>2</sub> splitting activity of the coated and virgin ceria foams

As previously unveiled, fuel production from LSMMg-CeO<sub>2</sub> foam is very sensitive to the operating conditions. Thus, the following parameters: reduction temperature at 1400°C under 0.100 bar, oxidation step starting at 1050°C with CO<sub>2</sub> molar fraction of 1.00 and total gas flow of 2.0 L/min were selected as “optimal conditions”. A comparison of LSMMg-CeO<sub>2</sub> foam with pure CeO<sub>2</sub> foam in the optimal conditions is presented in Figure 7. The CO cumulative production for both foams is provided in Figure 8. As for the reference conditions (Fig. S6), the LSMMg-CeO<sub>2</sub> foam reaches a higher reduction extent (220 μmol/g) than pure CeO<sub>2</sub> foam (154 μmol/g). During the oxidation step, the LSMMg-CeO<sub>2</sub> foam exhibits a lower fuel production rate (4.6 mL/g/min) as well as a lower re-oxidation extent (87%) than the pure CeO<sub>2</sub> foam (7.5 mL/g/min and 100%, respectively). The time required to reach 90% of the maximum CO production yield is also significantly longer for LSMMg-CeO<sub>2</sub> (5.8 min) than for pure CeO<sub>2</sub> foam (2.0 min), as evidenced in Fig. 8. However, the CO production yield is significantly higher for LSMMg-CeO<sub>2</sub> foam (387 μmol/g) than for pure CeO<sub>2</sub> foam (341 μmol/g). The LSMMg coating thus permits to increase the amount of fuel produced, but it also tends to slow the production rate in comparison with uncoated ceria foam.

A key parameter for future industrial implementation of the two-step thermochemical cycles is the solar-to-fuel conversion efficiency. The peak solar-to-fuel conversion efficiency (as defined in [38]) and the global cycle energy conversion efficiency (ratio of total heat value of produced fuel to heat consumed for reactant heating and endothermic reduction enthalpy) were assessed. In the case of LSMMg-CeO<sub>2</sub> foam, it is assumed that the reduction enthalpy is the weighted sum of the reduction enthalpy of CeO<sub>2</sub> and LSMMg (i.e. 439 kJ/mol and 243 kJ/mol for  $\delta=0.078$ , respectively). The reduction enthalpy of pure CeO<sub>2</sub> is taken at 453 kJ/mol for  $\delta=0.052$  [18, 41]. The cycle #3 for LSMMg-CeO<sub>2</sub> foam reaches a global cycle energy conversion efficiency of 3.7% and a peak solar-to-fuel conversion efficiency of 5.3%. In comparison, for similar operating conditions, the CeO<sub>2</sub> foam achieves cycle energy conversion efficiency and peak solar-to-fuel conversion efficiency of 3.4% and 5.5%, respectively. These efficiencies are close to those of the LSMMg-CeO<sub>2</sub> foam. Thus, the LSMMg coating does not impact on the efficiency of the ceria foam. Overall, this study thus revealed for the first time that LSMMg-CeO<sub>2</sub> composite foam displays synergistic oxygen release during the reduction step with a higher total fuel production compared to pure ceria, and similar energy conversion efficiency as ceria. Consequently, the use of a perovskite layer was shown to enhance the performance of ceria for thermochemical water splitting and CO<sub>2</sub> reduction cycles. After the series of cycles performed, the foam shape and dimensions remained intact in the cavity, although the structure was more brittle than the original one but the thermomechanical integrity was not altered.

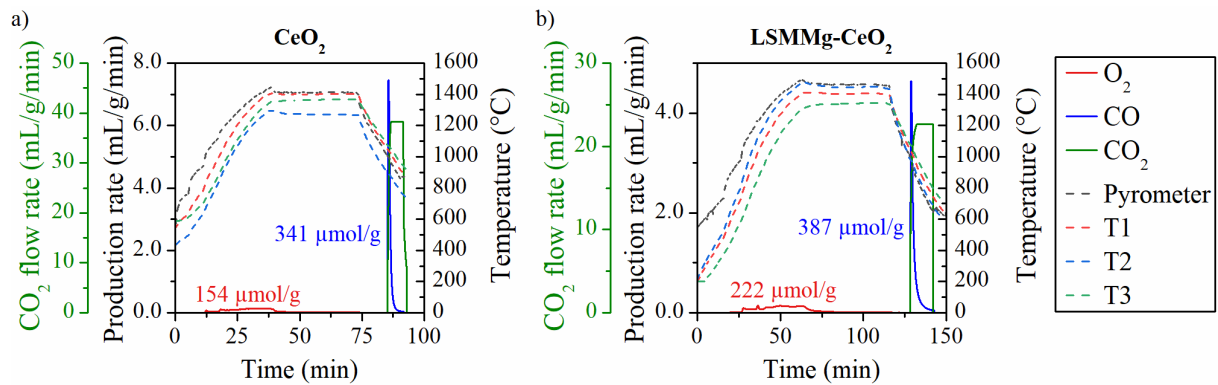


Figure 7. Thermochemical cycles performed with T1~1400°C under 0.100 bar (reduction step), followed by oxidation at 1050°C under 100% CO<sub>2</sub> for a) CeO<sub>2</sub> foam and b) LSMMg-CeO<sub>2</sub> composite foam (Cycle #3).

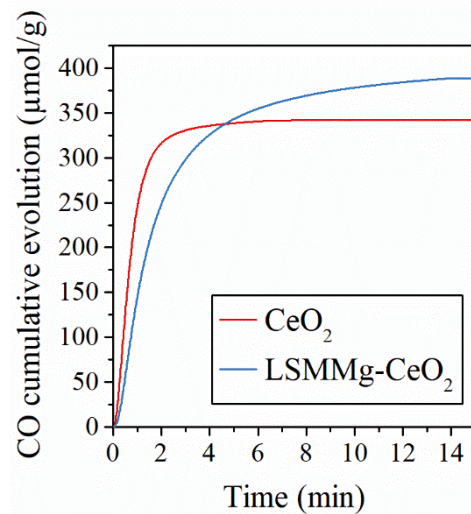


Figure 8. CO cumulative evolution for pure CeO<sub>2</sub> foam and LSMMg-CeO<sub>2</sub> foam during oxidation at 1050°C under 100% CO<sub>2</sub> (for reduction step performed with T1~1400°C under 0.100 bar)

#### 4. Conclusion

The thermochemical cycling performance of ceria foam coated with LSMMg perovskite layer (~10 μm thick) was studied in a solar reactor. The LSMMg coating was found to enhance the reduction extent reached by the reactive material compared with uncoated ceria foam. The re-oxidation yield of LSMMg-CeO<sub>2</sub> foam tended to be lower than the one measured for a pure CeO<sub>2</sub> foam presumably due to the diffusional barrier effect of LSMMg coating, limiting the access of oxidant species to the ceria bulk. However, a relevant tuning of the operating parameters was found to improve drastically the LSMMg-CeO<sub>2</sub> foam performance. Especially, a low pressure during the reduction step improved the reduction extent, and in turn the fuel production yield. During the oxidation step, a high oxidant molar fraction enhanced the re-oxidation extent. Increasing the total gas flow rate while maintaining the oxidant molar fraction offered beneficial impact on the fuel production rate. With such optimized operating conditions, the LSMMg-CeO<sub>2</sub> foam provided a higher fuel production yield in comparison with pure CeO<sub>2</sub> foam, despite a lower fuel production rate. In the next future, an optimization of coating layer porosity will be considered for improving the access of oxidant species to the bulk ceria

and thus reaching higher fuel production rate, since the oxidation step is a surface-controlled reaction. Furthermore, composite dual-phase foams containing a dispersion of the perovskite phase promoter within ceria should be considered for synergistic enhancement of oxygen exchange during reduction while avoiding oxidation rate limitation.

## Conflicts of interest

There are no conflicts to declare

## 5. Acknowledgments

This work was funded by the French National Agency for Research (ANR, SUNFUEL project, contract N°ANR-16-CE06-0010). The authors thank R. Garcia (PROMES) for solar reactor design, V. Bollee and J. Valls (Alsys-CTI) for supplying the raw ceria foams.

## Supplementary Information

Materials synthesis: perovskite powder synthesis, ceramic suspension, ceria foams coating, potential interactions between fluorite and perovskite phases, materials microstructure. Thermochemical redox cycling and fuel production performance.

## 6. References

- [1] Z. Şen, *Solar Energy Fundamentals and Modeling Techniques*. London: Springer London, 2008.
- [2] E. Kabir, P. Kumar, S. Kumar, A. A. Adelodun, and K.-H. Kim, “Solar energy: Potential and future prospects,” *Renew. Sustain. Energ. Rev.*, vol. 82, pp. 894–900, 2018.
- [3] V. Smil, *Energy transitions: global and national perspectives*, Second edition. Santa Barbara, California: Praeger, an imprint of ABC-CLIO, LLC, 2017.
- [4] A. Haeussler, S. Abanades, J. Jouannaux, M. Drobek, A. Ayril, and A. Julbe, “Recent progress on ceria doping and shaping strategies for solar thermochemical water and CO<sub>2</sub> splitting cycles,” *AIMS Mater. Sci.*, vol. 6, no. 5, pp. 657–684, 2019.
- [5] D. Arifin, A. Ambrosini, S. A. Wilson, B. Mandal, C. L. Muhich, and A. W. Weimer, “Investigation of Zr, Gd/Zr, and Pr/Zr – doped ceria for the redox splitting of water,” *Int. J. Hydrogen Energy*, vol. 45, no. 1, pp. 160–174, 2020.
- [6] R. R. Bhosale, G. Takalkar, P. Sutar, A. Kumar, F. AlMamani, and M. Khraisheh, “A decade of ceria based solar thermochemical H<sub>2</sub>O/CO<sub>2</sub> splitting cycle,” *Int. J. Hydrogen Energy*, vol. 44, no. 1, pp. 34–60, 2019.
- [7] A. Le Gal and S. Abanades, “Catalytic investigation of ceria-zirconia solid solutions for solar hydrogen production,” *Int. J. Hydrogen Energy*, vol. 36, no. 8, pp. 4739–4748, 2011.
- [8] A. Haeussler, S. Abanades, J. Jouannaux, and A. Julbe, “Non-Stoichiometric Redox Active Perovskite Materials for Solar Thermochemical Fuel Production: A Review,” *Catalysts*, vol. 8, no. 12, pp. 611–631, 2018.
- [9] M. Ezbiri, M. Takacs, D. Theiler, R. Michalsky, and A. Steinfeld, “Tunable thermodynamic activity of La<sub>x</sub>Sr<sub>1-x</sub>Mn<sub>y</sub>Al<sub>1-y</sub>O<sub>3-δ</sub> (0 ≤ x ≤ 1, 0 ≤ y ≤ 1) perovskites for solar thermochemical fuel synthesis,” *J. Mater. Chem. A*, vol. 5, no. 8, pp. 4172–4182, 2017.

- [10] L. Wang, M. Al-Mamun, P. Liu, Y. Wang, H. G. Yang, and H. Zhao, "Notable hydrogen production on  $\text{La}_x\text{Ca}_{1-x}\text{CoO}_3$  perovskites via two-step thermochemical water splitting," *J. Mater. Sci.*, vol. 53, no. 9, pp. 6796–6806, 2018.
- [11] M. M. Nair and S. Abanades, "Experimental screening of perovskite oxides as efficient redox materials for solar thermochemical  $\text{CO}_2$  conversion," *Sustainable Energy Fuels*, vol. 2, no. 4, pp. 843–854, 2018.
- [12] M. Orfila, M. Linares, R. Molina, J. Á. Botas, R. Sanz, and J. Marugán, "Perovskite materials for hydrogen production by thermochemical water splitting," *Int. J. Hydrogen Energy*, vol. 41, no. 42, pp. 19329–19338, 2016.
- [13] L. Wang, M. Al-Mamun, Y. L. Zhong, P. Liu, Y. Wang, H. G. Yang, and H. Zhao, "Enhanced Thermochemical Water Splitting through Formation of Oxygen Vacancy in  $\text{La}_{0.6}\text{Sr}_{0.4}\text{BO}_{3-\delta}$  (B=Cr, Mn, Fe, Co, and Ni) Perovskites," *ChemPlusChem*, vol. 83, no. 10, pp. 924–928, 2018.
- [14] A. H. Bork, M. Kubicek, M. Struzik, and J. L. M. Rupp, "Perovskite  $\text{La}_{0.6}\text{Sr}_{0.4}\text{Cr}_{1-x}\text{Co}_x\text{O}_{3-\delta}$  solid solutions for solar-thermochemical fuel production: strategies to lower the operation temperature," *J. Mater. Chem. A*, vol. 3, no. 30, pp. 15546–15557, 2015.
- [15] A. Demont, S. Abanades, and E. Beche, "Investigation of Perovskite Structures as Oxygen-Exchange Redox Materials for Hydrogen Production from Thermochemical Two-Step Water-Splitting Cycles," *J. Phys. Chem. C*, vol. 118, no. 24, pp. 12682–12692, 2014.
- [16] T. Khamhangdatepon, V. Tongnan, M. Hartley, T. Sornchamni, N. Siri-Nguan, N. Laosiripojana, K. Li, and U. W. Hartley, "Mechanisms of synthesis gas production via thermochemical cycles over  $\text{La}_{0.3}\text{Sr}_{0.7}\text{Co}_{0.7}\text{Fe}_{0.3}\text{O}_3$ ," *Int. J. Hydrogen Energy*, 2020.
- [17] J. R. Scheffe, D. Weibel, and A. Steinfeld, "Lanthanum–Strontium–Manganese perovskites as redox materials for solar thermochemical splitting of  $\text{H}_2\text{O}$  and  $\text{CO}_2$ ," *Energ. Fuel*, vol. 27, no. 8, pp. 4250–4257, 2013.
- [18] C.-K. Yang, Y. Yamazaki, A. Aydin, and S. M. Haile, "Thermodynamic and kinetic assessments of strontium-doped lanthanum manganite perovskites for two-step thermochemical water splitting," *J. Mater. Chem. A*, vol. 2, no. 33, pp. 13612–13623, 2014.
- [19] C. Agrafiotis, M. Roeb, and C. Sattler, "A review on solar thermal syngas production via redox pair-based water/carbon dioxide splitting thermochemical cycles," *Renew. Sustain. Energ. Rev.*, vol. 42, pp. 254–285, 2015.
- [20] A. H. Bork, E. Povoden-Karadeniz, and J. L. M. Rupp, "Modeling Thermochemical Solar-to-Fuel Conversion: CALPHAD for Thermodynamic Assessment Studies of Perovskites, Exemplified for  $(\text{La},\text{Sr})\text{MnO}_3$ ," *Adv. Energy Mater.*, vol. 7, no. 1, p. 1601086, 2017.
- [21] J. H. Kuo, H. U. Anderson, and D. M. Sparlin, "Oxidation-reduction behavior of undoped and Sr-doped  $\text{LaMnO}_3$  nonstoichiometry and defect structure," *J. Solid State Chem.*, vol. 83, no. 1, pp. 52–60, 1989.
- [22] M. E. Gálvez, R. Jacot, J. Scheffe, T. Cooper, G. Patzke, and A. Steinfeld, "Physico-chemical changes in Ca, Sr and Al-doped La–Mn–O perovskites upon thermochemical splitting of  $\text{CO}_2$  via redox cycling," *Phys. Chem. Chem. Phys.*, vol. 17, no. 9, pp. 6629–6634, 2015.
- [23] R. Carrillo and J. R. Scheffe, "Beyond Ceria: Theoretical Investigation of Isothermal and Near-Isothermal Redox Cycling of Perovskites for Solar Thermochemical Fuel Production," *Energ. Fuel*, 2019.
- [24] N. Gokon, K. Hara, Y. Sugiyama, S. Bellan, T. Kodama, and C. Hyun-seok, "Thermochemical two-step water splitting cycle using perovskite oxides based on  $\text{LaSrMnO}_3$  redox system for solar  $\text{H}_2$  production," *Thermochim. Acta*, vol. 680, p. 178374, 2019.
- [25] A. Demont and S. Abanades, "Solar thermochemical conversion of  $\text{CO}_2$  into fuel via two-step redox cycling of non-stoichiometric Mn-containing perovskite oxides," *J. Mater. Chem. A*, vol. 3, no. 7, pp. 3536–3546, 2015.

- [26] D. Maiti, B. J. Hare, Y. A. Daza, A. E. Ramos, J. N. Kuhn, and V. R. Bhethanabotla, "Earth abundant perovskite oxides for low temperature CO<sub>2</sub> conversion," *Energy Environ. Sci.*, vol. 11, no. 3, pp. 648–659, 2018.
- [27] C. N. R. Rao and S. Dey, "Generation of H<sub>2</sub> and CO by solar thermochemical splitting of H<sub>2</sub>O and CO<sub>2</sub> by employing metal oxides," *J. Solid State Chem.*, vol. 242, pp. 107–115, 2016.
- [28] M. Ezbiri, "Design of perovskite redox materials for the thermochemical splitting of H<sub>2</sub>O and CO<sub>2</sub> and for O<sub>2</sub> separation," ETH Zurich, 2017.
- [29] J. Jouannaux, A. Haeussler, M. Drobek, A. Ayrál, S. Abanades, and A. Julbe, "Lanthanum manganite perovskite ceramic powders for CO<sub>2</sub> splitting: Influence of Pechini synthesis parameters on sinterability and reactivity," *Ceram. Int.*, vol. 45, no. 12, pp. 15636–15648, 2019.
- [30] H. S. Cho, T. Myojin, S. Kawakami, N. Gokon, T. Kodama, Y. H. Kang, S. N. Lee, K. K. Chai, H. K. Yoon, and H. J. Lee, "Solar Demonstration of Thermochemical Two-step Water Splitting Cycle Using CeO<sub>2</sub>/MPSZ Ceramic foam Device by 45kW<sub>th</sub> KIER Solar Furnace," *Energy Procedia*, vol. 49, pp. 1922–1931, 2014.
- [31] H. S. Cho, N. Gokon, T. Kodama, Y. H. Kang, and H. J. Lee, "Improved operation of solar reactor for two-step water-splitting H<sub>2</sub> production by ceria-coated ceramic foam device," *Int. J. Hydrogen Energy*, vol. 40, no. 1, pp. 114–124, 2015.
- [32] B. J. Hathaway, R. Bala Chandran, A. C. Gladen, T. R. Chase, and J. H. Davidson, "Demonstration of a Solar Reactor for Carbon Dioxide Splitting via the Isothermal Ceria Redox Cycle and Practical Implications," *Energ. Fuel*, vol. 30, no. 8, pp. 6654–6661, 2016.
- [33] D. Marxer, P. Furler, M. Takacs, and A. Steinfeld, "Solar thermochemical splitting of CO<sub>2</sub> into separate streams of CO and O<sub>2</sub> with high selectivity, stability, conversion, and efficiency," *Energ. Environ. Sci.*, vol. 10, no. 5, pp. 1142–1149, 2017.
- [34] R. B. Diver, J. E. Miller, N. P. Siegel, and T. A. Moss, "Testing of a CR5 Solar Thermochemical Heat Engine Prototype," in *ASME 2010 4th International Conference on Energy Sustainability, Volume 2*, Phoenix, Arizona, USA, pp. 97–104, 2010.
- [35] J. E. Miller, M. D. Allendorf, A. Ambrosini, K. S. Chen, E. N. Coker, D. E. Dedrick, R. Diver, R. E. Hogan, I. Ermanoski, T. A. Johansson, G. L. Kellogg, A. H. McDaniel, N. Siegel, C. L. Staiger, and E. B. Stechel, "Reimagining Liquid Transportation Fuels: Sunshine to Petrol," Sandia National Laboratories, USA, SAND2012-0307, 2012.
- [36] H. I. Villafán-Vidales, C. A. Arancibia-Bulnes, D. Riveros-Rosas, H. Romero-Paredes, and C. A. Estrada, "An overview of the solar thermochemical processes for hydrogen and syngas production: Reactors, and facilities," *Renew. Sustain. Energ. Rev.*, vol. 75, pp. 894–908, 2017.
- [37] F. A. Costa Oliveira, M. A. Barreiros, S. Abanades, A. P. F. Caetano, R. M. Novais, and R. C. Pullar, "Solar thermochemical CO<sub>2</sub> splitting using cork-templated ceria ecoceramics," *J. CO<sub>2</sub> Util.*, vol. 26, pp. 552–563, 2018.
- [38] A. Haeussler, S. Abanades, A. Julbe, J. Jouannaux, M. Drobek, A. Ayrál, and B. Cartoixa, "Remarkable performance of microstructured ceria foams for thermochemical splitting of H<sub>2</sub>O and CO<sub>2</sub> in a novel high-temperature solar reactor," *Chem. Eng. Res. Des.*, vol. 156, pp. 311–323, 2020.
- [39] A. Haeussler, S. Abanades, F. Oliveira, M. A. Barreiros, A. P. Caetano, R. Novais, and R. C. Pullar, "Solar redox cycling of ceria structures based on fiber boards, foams and biomimetic cork-derived ecoceramics for two-step thermochemical H<sub>2</sub>O and CO<sub>2</sub> splitting," *Energy & Fuels*, 2020. In Press. DOI: 10.1021/acs.energyfuels.0c01240
- [40] P. Nikolaidis and A. Poullikkas, "A comparative overview of hydrogen production processes," *Renew. Sustain. Energ. Rev.*, vol. 67, pp. 597–611, 2017.
- [41] R. J. Panlener, R. N. Blumenthal, and J. E. Garnier, "A thermodynamic study of nonstoichiometric cerium dioxide," *J. Phys. Chem. Solids*, vol. 36, no. 11, pp. 1213–1222, 1975.